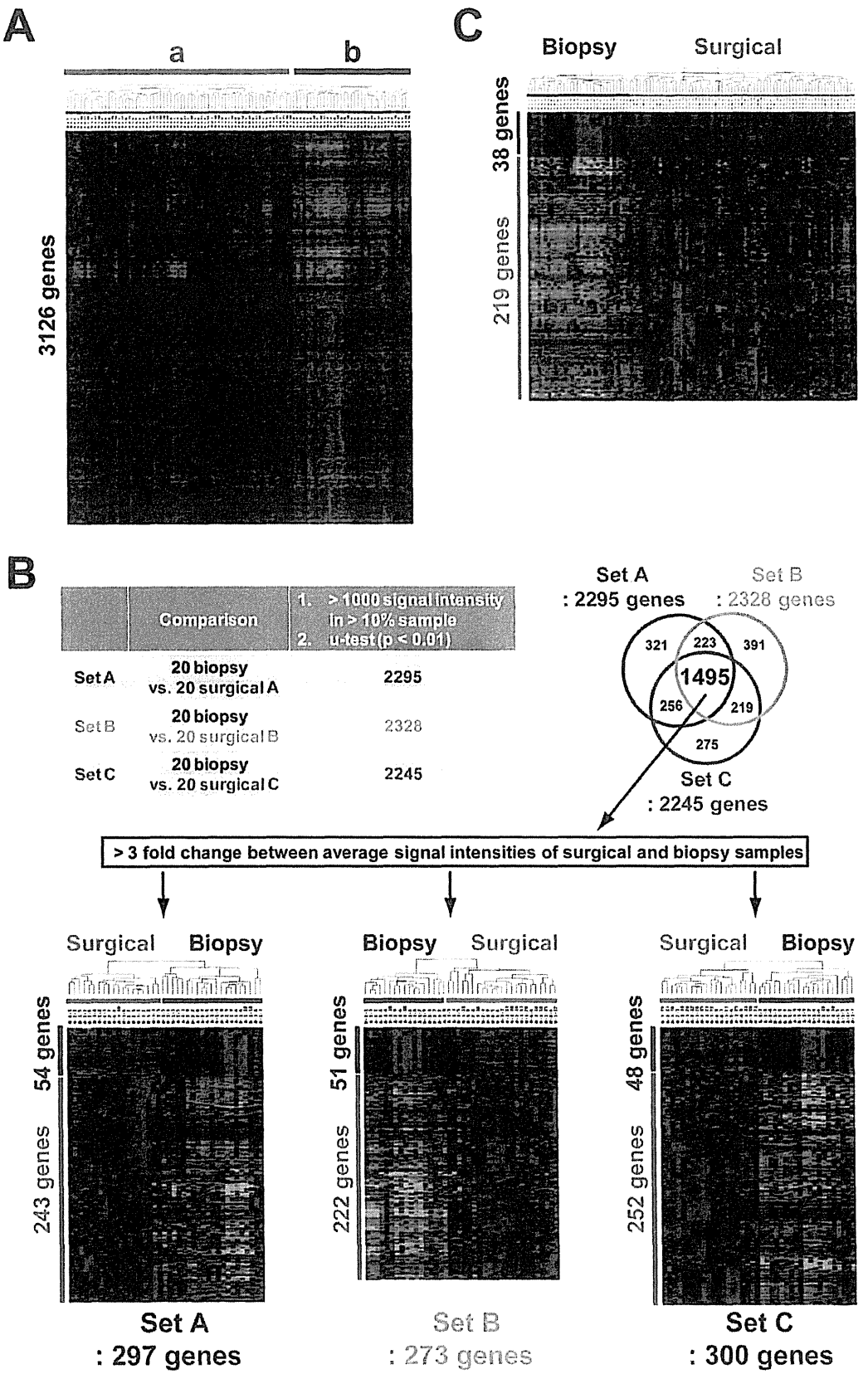
A
a
b
3126 genes
C
Biopsy
Surgical
38 genes
219 genes
B
Comparison
1. > 1000 signal intensity in > 10% sample
2. u-test (p < 0.01)
Set A
20 biopsy vs. 20 surgical A
2295
Set B
20 biopsy vs. 20 surgical B
2328
Set C
20 biopsy vs. 20 surgical C
2245
Set A : 2295 genes
Set B : 2328 genes
321
223
391
1495
256
219
275
Set C : 2245 genes
> 3 fold change between average signal intensities of surgical and biopsy samples
Surgical
Biopsy
54 genes
243 genes
Set A : 297 genes
Biopsy
Surgical
51 genes
222 genes
Set B : 273 genes
Surgical
Biopsy
48 genes
252 genes
Set C : 300 genes

Figure 1. Comparison of expression profiles between biopsy and surgically resected esophageal tumor samples obtained from different cases. (A) Unsupervised clustering with 3,126 processed genes. Surgical (a) and biopsy sample clusters (b) are shown. (B) Comparison of expression profiles among three independent sets (A, B, and C): a randomly selected 20-biopsy sample set versus three surgical sample sets (A, B, and C) containing 20 independent cases. The number of differentially expressed genes selected by u-test ($p<0.01$): 2, 295 in set A, 2,328 in set B, and 2, 245 in set C (Upper). The number of differentially expressed genes with a 3-fold change between two average signal intensities: 297, 273, and 300. Clustering results with these gene sets (Lower). (C) Up-regulated genes in surgical or biopsy samples. By the use of all of the profiles under stringent selection conditions (see Materials and Methods), 38 and 219 genes were identified as up-regulated genes in the biopsy and surgical samples, respectively.
doi:10.1371/journal.pone.0018196.g001

4 hours after resection revealed that mouse *Zeb1*, *Zeb2*, *Vim*, and *Fn* were induced 4 hours after resection (Figure 6B, lower). Quantitative real-time RT-PCR confirmed over-expression of *Zeb1*, *Zeb2*, *Vim*, and *Fn* after resection (Figure 6C). Since overall sensitivity of mouse affymetrix arrays is known to be lower than in humans, and the use of a small amount of RNA such as laser-captured subjects is also known to reduce microarray sensitivity, *Twist1* mRNA itself could not be detected in this mouse experiment (data not shown).

To investigate whether aiEMT in the mRNA levels affects IHC, we performed IHC on a typical mesenchymal marker vimentin 8 hours after resection. Here we determined conditions under which normal epithelial cell layers are stained. In all of the 3 independent samples examined, normal epithelial cell layers were not found to be stained highly 8 hours after resection (Figures 7A–C). The discrepancy between the mRNA level and protein level can be explained by the two following reasons: 1) although undifferentiated layers (basal and parabasal) have been reported to express EMT-related genes including *VIM* [4], their expression levels were much lower than tumor (Figure 5B). 2) it may also be difficult to show the approximate 2-fold change in the mRNA level (Figures 6B, C) as in the protein level by IHC, because IHC is inferior to RT-PCR in both sensitivity and quantification.

All of the results suggest that EMT, especially in the mRNA level, is induced artificially in both normal and malignant epithelial cells by surgical resection-related events (ischemia-induced hypoxia and hyponutrition, and hypoxia-induced inflammation, etc.).

Artificially Induced EMT (aiEMT) by Surgical Resection Prevents Microarray-based Subgroup Identification

Identification of clinically significant subgroups is very important for personalized medicine and for drug development against intractable cases. When we used the expression profiles of the 35 biopsy samples obtained from patients treated by chemoradiotherapy [8], unsupervised clustering with 5,570 processed genes (Materials and Methods) identified a good responder group consisting of 9 patients (7/9, 78% showing complete response to chemoradiotherapy) from the 35 (Figure 8A, left). However, when the profiles of the 66 surgical samples were used, unsupervised clustering with 2,016 processed genes could not identify any subgroup (Figure 8A, right). Thus, biopsy sample expression profiles seemed to be more effective in subgroup identification than those of the surgical samples. In fact, we previously reported that biopsy sample expression profiles could distinguish long-term or short-term survivors by definitive chemoradiotherapy [8]; however, surgical sample expression profiles never identified poor prognostic subgroups with extensive lymph node metastasis [10]. Moreover, in the surgical samples, EMT was accelerated in 36 (85.7%) out of 42 esophageal cancers [9]. This high percentage seems to be caused by aiEMT.

To address the reason why subgrouping is difficult in surgical samples, we compared the number and distribution of each of the processed genes, which were used for unsupervised clustering. We first selected genes with a signal intensity of more than 1,000 in more than 10% of the samples. From 35 biopsy and 66 surgical samples, 6,551 and 4,797 genes, respectively, were selected. From these genes, we finally selected more than 3-fold changed genes by comparing the average signal intensity of each gene in more than 10% of the samples. In the 35 biopsy samples, 85% (5,570) of 6,551 first processed genes remained, whereas the number of final processed genes decreased from 4,797 first processed genes to 2,016 (42%) (Figure 8B, upper). Of the 2,016 finally processed genes in the surgical samples, 1,724 (86%) were included in the 5,570 finally processed genes in the biopsy samples; however, 3,846 (69%) of 5,570 genes were unique to the biopsy samples (Figure 8B, lower). Moreover, frequency distribution (for percentage of samples) of these two finally processed-gene sets shows that approximately 60% of the 2,016 processed genes in the surgical samples express in only a limited number of cases (0–10%) (Figure 8C). Accordingly, aiEMT in surgical samples may diminish the number of processed genes useful for subgroup identification.

Discussion

We recently reported the presence of crosstalk between Hedgehog (Hh) and EMT signaling in normal and malignant epithelial cells of the esophagus [9]. In that report, *ZEB2* was shown to be a downstream gene of both a primary transcriptional transducer GLI1 in Hh signaling and of another EMT regulator, TWIST1, and that ZEB2 further up-regulated 5 chemokine or growth factor receptors, *PDGFRA*, *EDNRA*, *CXCR4*, *VEGFR2*, and *TRKB* (Figure S4). The Hh signal block inhibited esophageal keratinocyte differentiation and cancer cell invasion and growth. Accordingly, over-expression of *ZEB2* and *TWIST1* in surgical samples of both normal and tumor tissues can induce EMT, resulting in over-expression of representative EMT markers *VIM*, *FN*, and *COLs* (Figures 2, 4, 6, S2, and S3) and membrane signal transducers *IL8*, *CXCL4*, *CCL5*, *CXCR4*, *PDGFRB*, and *TLR2* (Figure 2). Over-expression of the membrane signal transducers can activate further down-stream cascades. This is a major reason for the large difference of expression profiles between biopsy and surgical samples (Figures 1 and 3).

Extensive contamination of normal mesenchymal portions in surgically resected tumor tissues can also explain the over-expression of those EMT regulators and EMT-related genes, even though trained pathologists carefully excised bulk tissue samples from the main tumor, leaving a clear margin from the surrounding normal tissue (Materials and Methods). However, the over-expression was also observed in surgically resected normal tissue and mouse epithelial cell layers 4 hours after resection (Figure 6). Therefore, we concluded that artificially induced EMT, termed aiEMT, occurred in both normal and malignant epithelial cells by the surgical resection-related events (ischemia-induced hypoxia, ischemia-induced hyponutrition, and hypoxia-induced inflammation, etc.) (Figure S1).

Recently, the hypoxia-inducible factors (HIF-1A or HIF-2A) have been reported to directly regulate TWIST1 [13, 14] and

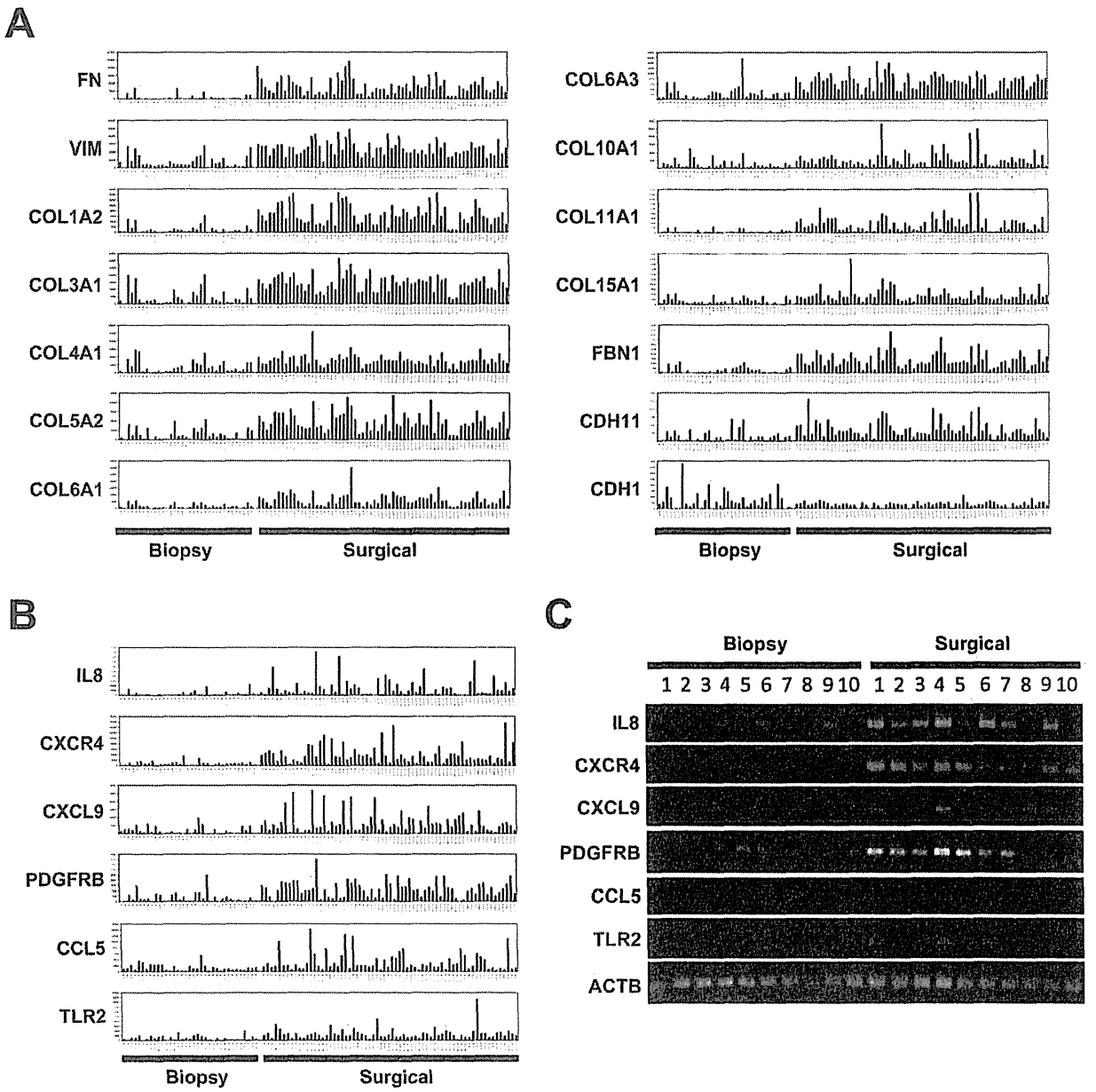

Figure 2. Representative EMT related genes over-expressed in surgically resected esophageal tumor samples. (A) Expression patterns of an epithelial cell marker E-cadherin (*CDH1*) and typical EMT markers including fibronectin (*FN*), vimentin (*VIM*), and collagens (*COLs*). (B) Expression patterns of 6 membrane signal transducers: a cytokine (*IL8*), two chemokines (*CXCL9* and *CCL5*), and three membrane type receptors (*CXCR4*, *PDGFRB*, and *TLR2*). (C) Semi-quantitative RT-PCR results of these 6 membrane transducers in representative samples.
doi:10.1371/journal.pone.0018196.g002

LOXL2, which reportedly stabilized an EMT regulator, SNAI1/SNAIL, through physical interaction on the SLUG domain and Snail's lysine residues K98 and K137 [15]. The SNAI1 binding site was also found in the 5' promoter region of *ZEB2* [16]. Over-expression of both *HIF1A* and *LOXL2* was observed only in the surgically resected tumor tissues obtained from different cases (Figure S5). Moreover, other *HIF1* families (*HIF1B* and *HIF2A*) were never over-expressed in any of the surgical samples. Therefore, elucidation of the molecular mechanisms of aiEMT in surgical samples remains for future studies. However, we noted that ischemia-induced hypoxia and/or inflammation has been reported to release repression of NFκB [17], which regulates *ZEB1*, *ZEB2*, and *TWIST1* [18, 19] and that TGF-β signaling may be involved in aiEMT, because over-expression of *NFKB1* and *TGFBR2* was found in surgical samples (Figure S6).

As mentioned in the Introduction, surgical samples have been used as important subjects for clinical and basic cancer research for many years. Therefore, aiEMT in surgical samples may have possibly interfered with or prevented not only microarray- or immunohistochemistry-based clinical research (diagnostic marker

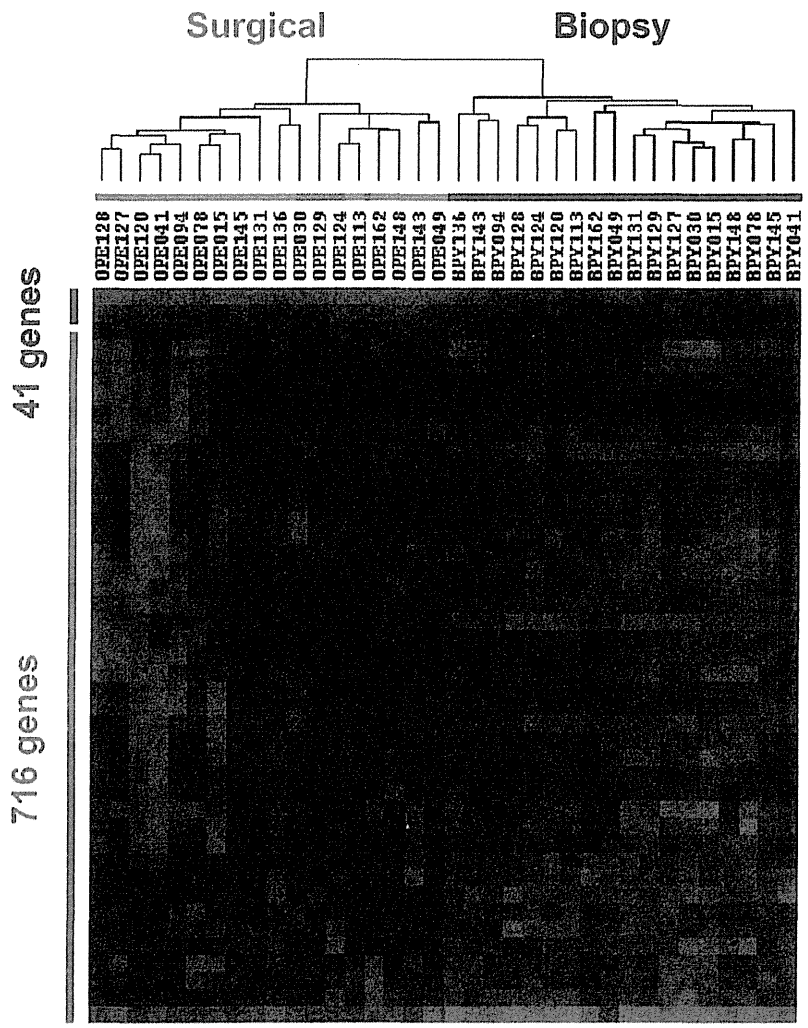

Figure 3. Up-regulated genes in biopsy and surgically resected esophageal tumor samples obtained from identical cases. By stringent selection (see Materials and Methods), 41 and 716 genes were identified as up-regulated genes in the biopsy and surgical samples, respectively.
doi:10.1371/journal.pone.0018196.g003

identification, subgrouping, making predictors, and prognosis evaluation, etc.) but also basic research (making a signal pathway map, therapeutic target identification, etc.). This study will likely evoke fundamental misinterpretation including underestimation of the prognostic evaluation power of markers by overestimation of EMT in past cancer research, and will provide some advice for the near future as follows: 1) Understanding how long the tissues were under an ischemic condition (from start of resection to stock or RNA preparation). The total amount of time should never exceed 4 hours. 2) Prevalence of biopsy samples for *in vivo* expression profiling with low biases on basic and clinical research; for example, for clinical outcome prediction of not only neoadjuvant but also adjuvant chemotherapy, radiotherapy, and chemoradiotherapy such as in previous reports [8, 20–23]. 3) Checking cancer cell contents and normal- or necrotic-tissue contamination in biopsy samples for the prevalence. In sampling by a needle biopsy, tumor portions (2mm X 2mm) should be obtained from a margin (periphery) of the tumor by exclusion of central necrotic lesions under endoscopy. If necrotic lesions were severely contaminated in the samples, those samples should be excluded by quantifying and qualifying RNA. If the samples contained extensive normal lesions, such samples can be excluded by the expression profile-based scoring method using normal and/or tumor specific genes.

Materials and Methods

Tissue Samples

All esophageal cancer (squamous cell carcinomas) and non-cancerous tissues were provided by the Central Hospital or East Hospital at the National Cancer Center after obtaining written informed consent from each patient and approval by the Center's Ethics Committee.

All surgical samples were obtained from patients without neoadjuvant therapy, and all biopsy samples were obtained before treatment. For the surgical samples, trained pathologists carefully excised bulk tissue samples from the main tumor, leaving a clear

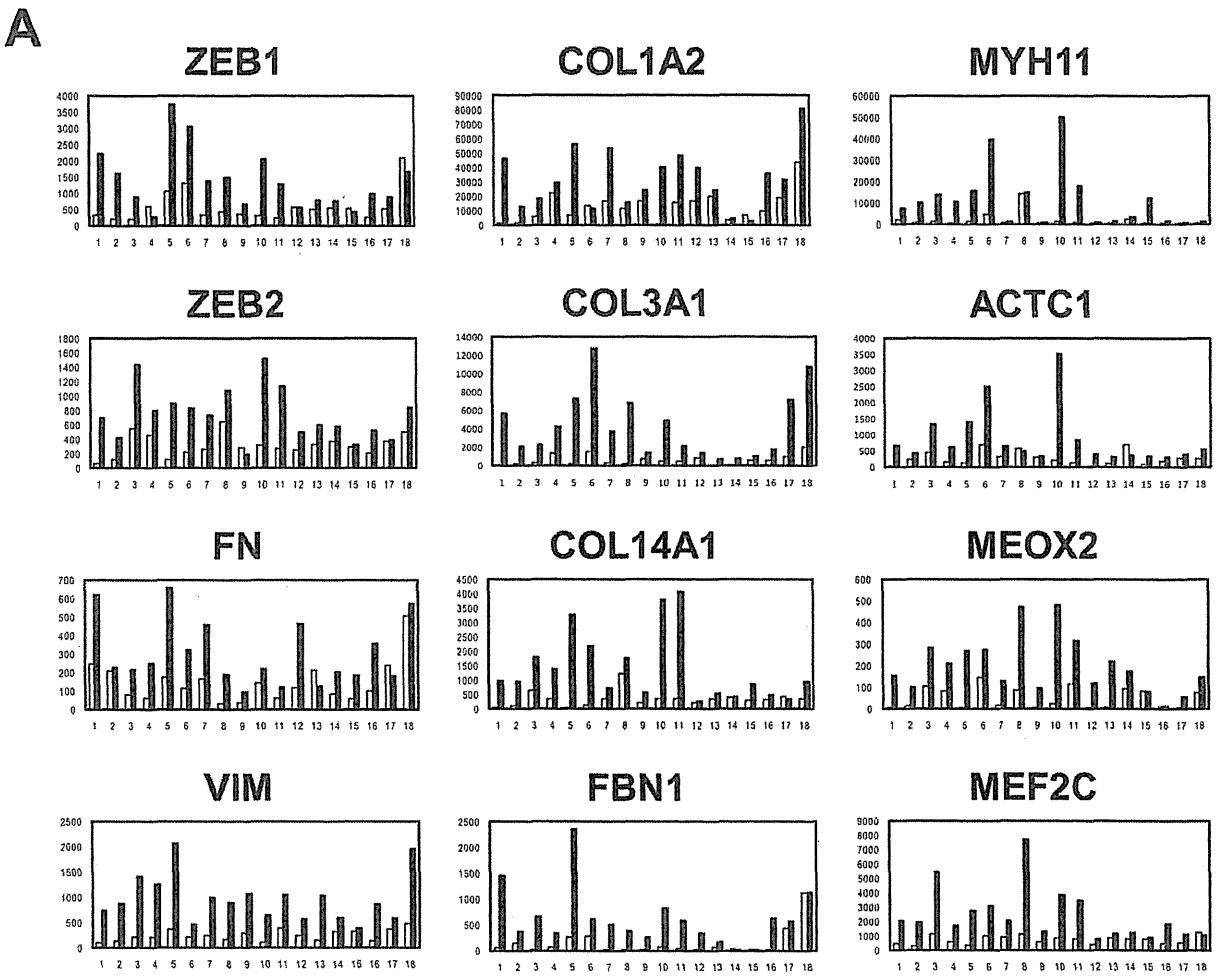
A
ZEB1
COL1A2
MYH11
ZEB2
COL3A1
ACTC1
FN
COL14A1
MEOX2
VIM
FBN1
MEF2C

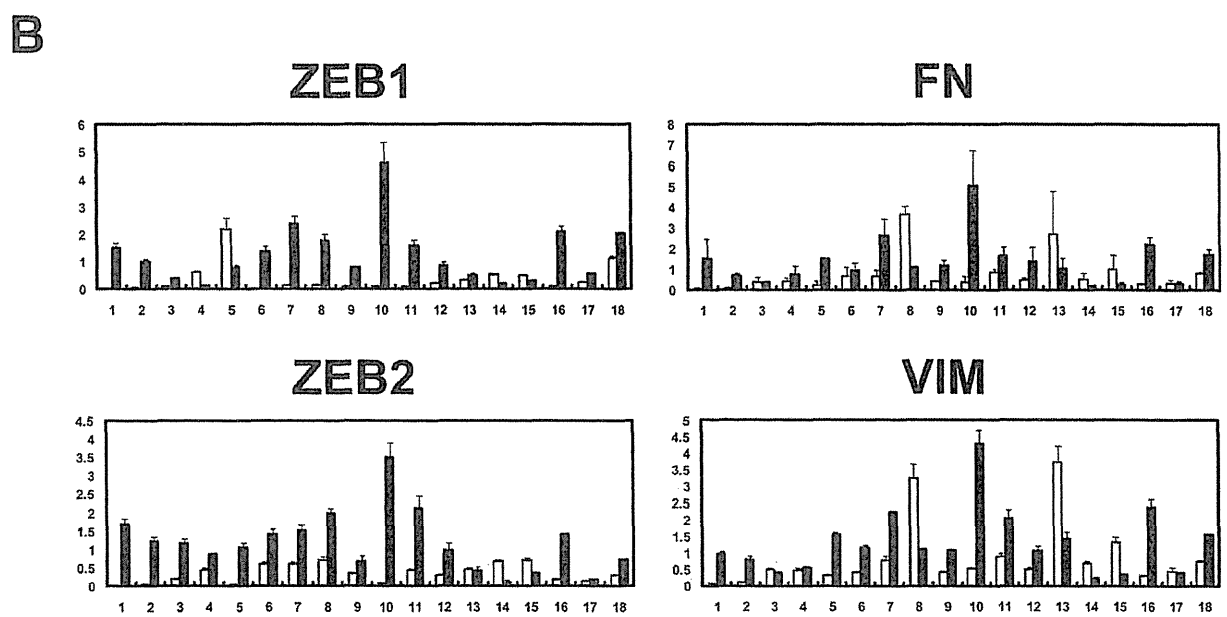
B
ZEB1
FN
ZEB2
VIM

Figure 4. Representative EMT related genes also over-expressed in surgically resected esophageal tumor samples obtained from identical cases. (A) Expression patterns of 2 representative EMT regulators (*ZEB1* and *ZEB2*), 8 typical EMT markers including fibronectin (*FN*), vimentin (*VIM*), 3 collagens (*COL1A2*, *COL3A1*, and *COL14A1*), *FBN1*, *MYH11*, and *ACTC1*, and 2 EMT-related myogenic transcription factors (*MEOX2* and *MEF2C*). (B) Quantitative real-time RT-PCR results of *ZEB1, ZEB2, FN, and VIM.* Closed box: surgical sample; Open box: biopsy sample.
doi:10.1371/journal.pone.0018196.g004

margin from the surrounding normal tissue. Thus, we obtained surgical samples from a margin (periphery) of the tumor. For the needle biopsy samples, tumor portions (2 mm X 2 mm) were obtained under endoscopy from a margin of the tumor by exclusion of any central necrotic lesions. If the samples were severely contaminated by necrotic lesions, those samples were excluded by quantifying and qualifying RNA. If the samples contained extensive normal lesions, we excluded such samples by

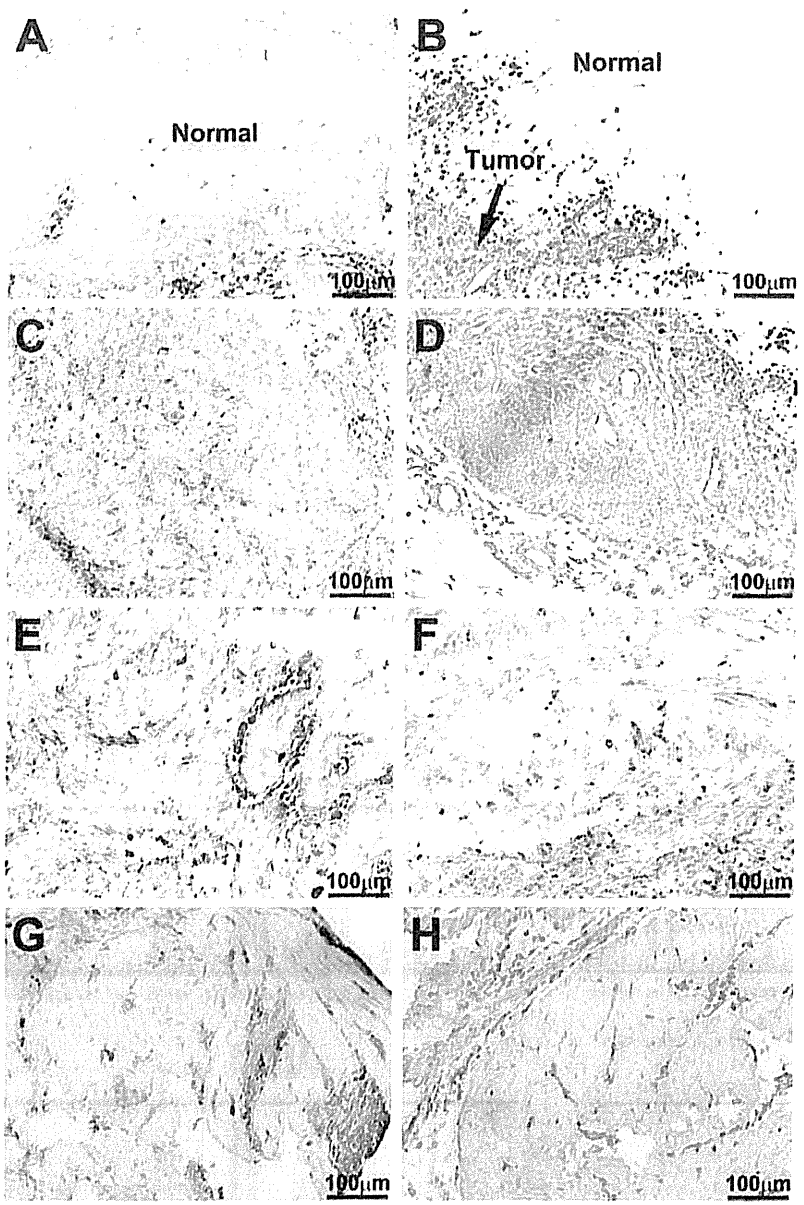

Figure 5. Immunohistochemistry (IHC) of a typical EMT marker vimentin in biopsy and surgically resected tissues. IHC of vimentin in an additional surgical sample, which contained normal portions, showed that normal esophageal epithelial cells were not stained, but invasive tumor cells were (A, B). In 3 out of 5 pairs of biopsy and surgical samples, over-expression of vimentin was observed in the surgical samples (biopsy: C, E, G; surgical: D, F, H).
doi:10.1371/journal.pone.0018196.g005

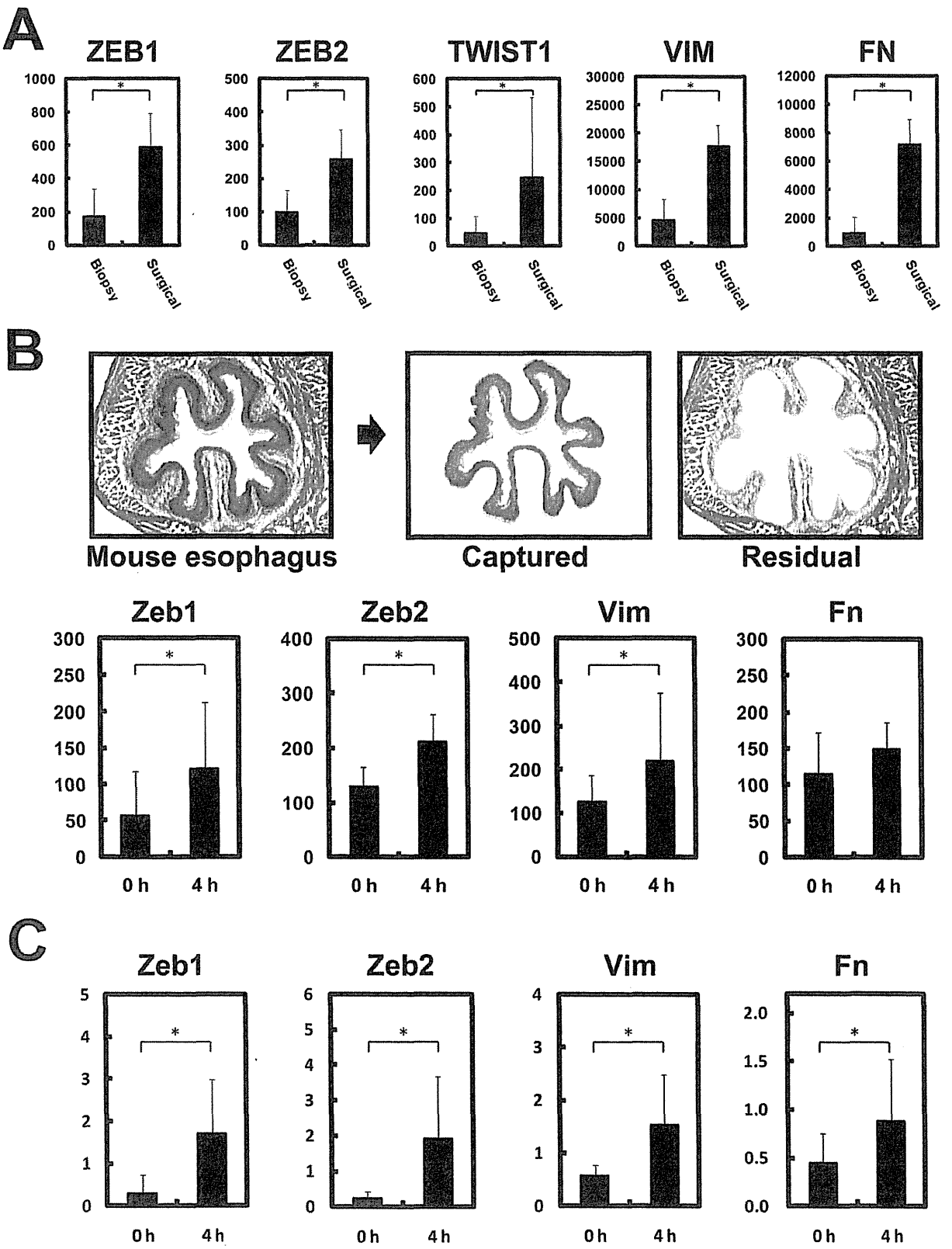
A
ZEB1
ZEB2
TWIST1
VIM
FN
Biopsy
Surgical
B
Mouse esophagus
Captured
Residual
Zeb1
Zeb2
Vim
Fn
0 h
4 h
C
Zeb1
Zeb2
Vim
Fn
0 h
4 h

Figure 6. Over-expression of EMT regulators and markers in surgically resected normal tissues. (A) Over-expression of EMT-regulators (*ZEB1*, *ZEB2*, and *TWIST1*) and EMT-markers (*VIM* and *FN*) in surgically resected normal esophagus mucosa. (B) Induction of mouse *Zeb1*, *Zeb2*, *Vim*, and *Fn* under ischemic condition. After resection of mouse esophagus, we placed it on PBS for 0 or 4 hours at room temperature (under an ischemic condition), immediately made frozen sections, captured the epithelial cell layer (upper) by laser microdissection, amplified mRNA by TALPAT [24–28], and obtained expression profiles using Mouse Expression Array 430 2.0 (Affymetrix, Santa Clara, CA). Experiments were performed on 3 mice. The *Zeb1*, *Zeb2*, *Vim*, and *Fn* genes are induced 4 hours after resection (Lower). *$P<0.05$. (C) Quantitative real time RT-PCR of *Zeb1*, *Zeb2*, *Vim*, and *Fn*. Over-expression of *Zeb1*, *Zeb2*, *Vim*, and *Fn*, shown by microarray, was confirmed.
doi:10.1371/journal.pone.0018196.g006

the expression profile-based scoring method using normal and/or tumor specific genes (in preparation).

The overall process of an esophageal cancer operation requires much time. Therefore, surgical samples were excised from a margin of the tumor by trained pathologists after exposure for 4–7 hours under an ischemic condition, and were immediately frozen at −80°C until use. On the contrary, needle biopsy samples resected under endoscopy were immediately frozen at −80°C until use. Clinicopathological information is given in Tables S3, S4, S5.

Laser Microdissection followed by RNA Extraction and Amplification

Cryostat sections (8μm) of frozen mouse esophageal samples were laser-microdissected with the mmi CellCut system (MMI Inc., Rockledge, FL). Total RNA was isolated by suspending the cells in an ISOGEN lysis buffer (Nippon Gene, Toyama, Japan) followed by precipitation with isopropanol. RNA was amplified by an efficient method of high-fidelity mRNA amplification, called TALPAT (T7 RNA polymerase promoter-attached, adaptor ligation-mediated, and PCR amplification followed by *in vitro* T7-transcription) [24–28].

Microarray Analysis

Gene expression profiles were obtained from 166 samples: tumor sets (different cases) of independent 35 and 20 biopsy samples and 66 surgical samples, another tumor set (identical case) of 18 biopsy samples and 18 surgical samples, a normal set of 4 biopsy samples and 5 surgical samples. Total RNAs extracted from the bulk tissue samples were biotin-labeled and hybridized to high-

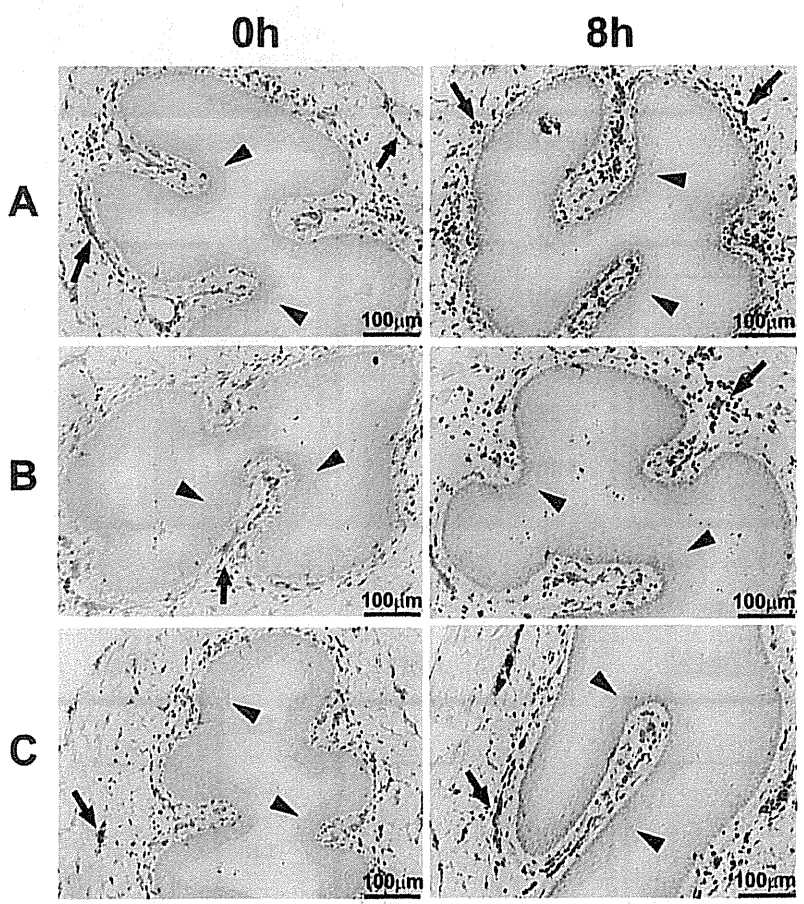

Figure 7. Immunohistochemistry (IHC) of a typical EMT marker vimentin in mouse esophagus. After resection of mouse esophagus, we placed it on PBS for 0, 4, 8 hours at room temperature (under an ischemic condition), immediately made frozen sections, and IHC of vimentin was performed under more sensitive conditions compared with Figure 5. Experiments were performed on 3 mice (A–C). Over-expression of vimentin in mouse esophageal epithelium was not observed even after 8 hours of exposure under an ischemic condition. Arrow: vimentin-positive smooth muscle, arrow head: mouse stratified esophageal epithelial cell layers.
doi:10.1371/journal.pone.0018196.g007

A

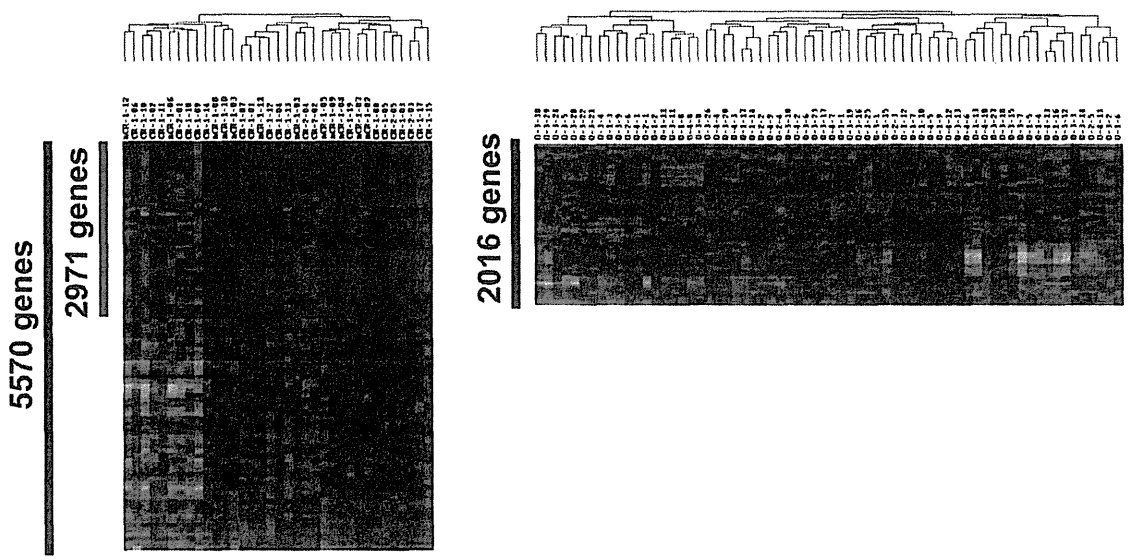

B

U95Av2 microarray data	1. > 1000 signal intensity in > 10% sample	1. > 1000 signal intensity in > 10% sample 2. > 3 fold change from Ave. intensity in > 10% sample
Biopsy 35 samples	6551	5570 (85%)
Surgical 66 samples	4797	2016 (42%)

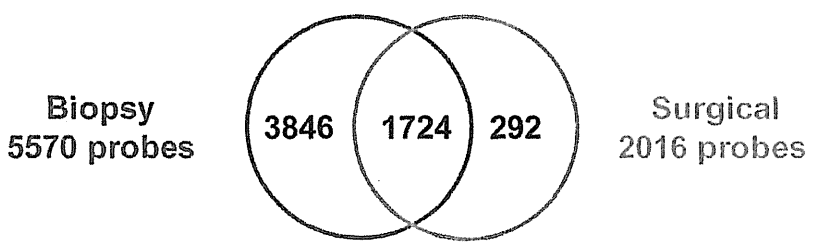

C

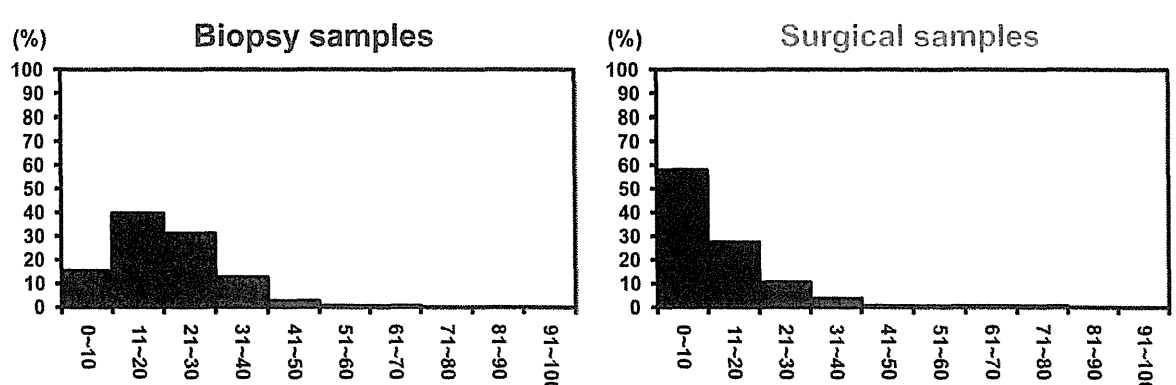

Figure 8. Artificially induced EMT prevents microarray-based subgroup identification. (A) Unsupervised clustering of 35 biopsy and 66 surgically resected esophageal tumor samples with 5,570 and 2,016 processed genes, respectively. A sample cluster with 2,971 genes appears only in the biopsy samples. (B) Comparison of the number of processed genes for unsupervised clustering between biopsy and surgical samples. The number of processed genes and commonly selected genes is indicated. (C) Frequency distribution for percentage of samples of finally processed-gene sets. Each distribution of 5, 570 genes in biopsy samples (Left) and 2,016 genes in surgical samples (Right) is indicated.
doi:10.1371/journal.pone.0018196.g008

density oligonucleotide microarrays (Human Genome U95Av2 or U133PLUS2.0 Array, Affymetrix, Santa Clara, CA, USA) in accordance with the manufacturer's instructions. For laser-captured mouse esophageal epithelial cell layers, Mouse Genome 430 2.0 Array was used. The scanned data of the arrays were processed by Affymetrix Microarray Suite version 4.0 or 5.0, which scaled the average intensity of all the genes on each array to a target signal of 1,000 to reliably compare variable multiple arrays. All the microarray data have been deposited in a MIAME compliant database, GEO; the accession number SuperSeries GSE22954.

Gene Selection from Microarray Data and Hierarchical Clustering

Hierarchical clustering is widely used as one of the unsupervised learning methods. Hierarchical clustering of microarray data was performed by the use of GeneSpring (Agilent Technologies Ltd., CA, USA), Microsoft EXCEL, and Cluster & TreeView software [29].For unsupervised clustering (Figures 1A and 8A), we first selected genes with a signal intensity of more than 1,000 in more than 10% of the samples, and from these genes, we finally selected more than 3-fold changed genes by comparing the average signal intensity of each gene in more than 10% of the samples. For overexpressed genes in the surgical or biopsy samples, we first selected genes by u-test ($p<0.01$), permutation test, and 2- or 3-fold change between the average signal intensities of the two sets of samples, and from the first selected genes we finally selected genes with more than 1,000 in average signal intensity.

Semi-quantitative and Quantitative RT-PCR

Total RNA was isolated by suspending the cells in Isogen lysis buffer (Nippon Gene, Toyama, Japan) followed by precipitation with isopropanol. RT-PCR was carried out using primer sets designed for detecting the 3′ side of cDNA of each human gene: for *IL8*, 5′- TGCCAAGGAGTGCTAAAG -3′ and 5′- CTCCACAACCCTCTGCAC-3′, for *CXCR4*, 5′-TGTATGTCTCGTGGTAGGAC-3′ and 5′-AGACTGTACACTGTAGGTGC-3′, for CXCL9, 5′-ACAAAGAAAATATTTCAAATTACAAGG-3′ and 5′-GGGAACGGTGAAGTACTAAGC-3′, for *PDGFRB*, 5′-ACTGCCCAGACCTAGCAGTG-3′ and 5′-CAGGGAAGTAAGGTGCCAAC-3′, for CCL5, 5′-CCCCGTGCCCACATCAAGGAGTATTT-3′ and 5′-CGTCCAGCCTGGGGAAGGTTTTTGTA-3′, for *TLR2*, 5′-CCAGCAGGAACATCTGCTAT-3′ and 5′-TCCAGGTAGGTCTTGGTGTT-3′, for *ZEB1*, 5′-CGTCTCTTTCAGCATCACCA-3′ and 5′-ATGGGAGACACCAAACCAAC-3′, for *ZEB2*, 5′-CATGACGTTGATCATTTGGGC-3′ and 5′-CGAGCATGGTCATTTTCAAAAG-3′, for *FN*, 5′-CGGGGGAAATAATTCCTGTG-3′ and 5′-CCTTGCAGGCAATCTCTTTG-3′, for *VIM*, 5′-GCTTTCAAGTGCCTTTCTGC-3′ and 5′-GTTGGTTGGATACTTGCTGG-3′, and for *ACTB* (β-actin), 5′-TCATCACCATTGGCAATGAG-3′ and 5′-CACTGTGTTGGCGTACAGGT-3′. Primer sets for detecting each mouse gene were also designed: for *Zeb1*, 5′-TAACATTTATACTTGCCTCC-3′ and 5′-GCTAAGGGAATGAGTTATGG-3′, for *Zeb2*, 5′-ACCAAATCAGACCACGAGGA-3′ and 5′-GCCCCTTCTGTCCCTCTCTA-3′, for *Fn*, 5′-CCGTGGGATGTTTTGAGACT-3′ and 5′-GGCAAAAGAAAGCAGAGGTG-3′, for *Vim*, 5′-ACGGTTGAGACCAGAGATGG-3′ and 5′-CGTCTTTTGGGGTGTCAGTT-3′ , and for *ActB*, 5′-GCTCTTTTCCAGCCTTCCTT-3′ and 5′-GTACTTGCGCTCAGGAGGAG-3′. For semi-quantitative RT-PCR, we showed data within linear range by performing 25–35 cycles of PCR. Quantitative real-time PCR was performed by a Bio-Rad iCycler with iQ Syber Green Supermix (Bio-Rad, Hercules, CA, USA) as directed by the manufacturer. The value of 1/2N (N: the number of PCR cycles corresponding to the onset of the linear amplification of each gene product) was calculated as a relative mRNA expression level of each gene normalized to *ACTB*. The data from 2 independent analyses for each sample were averaged.

Immunohistochemistry

For immunohistochemical staining of frozen sections of human and murine esophagus, specimens that were embedded in a TissueTek OCT medium (VWR Scientific Products, West Chester, CA) and stocked at −80°C until use were cut into 8μm sections, which were then left for 30 min at room temperature followed by fixing in 4% paraformaldehyde for 20 min at room temperature. Endogenous peroxidase activity was inhibited with 3% H_2O_2 in methanol for 30 min. Blocking was carried out with Vectastain ABC Elite Kit (Vector Laboratories, Burlingame, CA) for 30 min at room temperature. Sections were incubated for 60 min at room temperature with diluted mouse monoclonal antibody directed against human vimentin (N1521, DAKO, Carpinteria, CA) or rabbit polyclonal antibody directed against mouse vimentin (#3932, Cell Signaling Technology Japan, Tokyo, Japan). After washing sections with PBS, biotinylated secondary antibodies were applied for 30 min at room temperature. Detection was carried out by using Vectastain ABC Elite Kit (Vector Laboratories) and the DAB system (DAKO, Tokyo), and the sections were counter-stained with 1% Methyl Green. (Sigma, Saint Luis, MO)

Supporting Information

Figure S1 Schema of artificial factors during surgical resection and sample transportation. Biopsy samples are small, much fresher, with low contamination of normal portions compared to surgical samples, whereas some artificial factors such as ischemia, hypoxia, hyponutrition, and cold stress possibly occur during surgical resection and sample transportation.
(TIF)

Figure S2 Expression levels of *ZEB1* and *ZEB2* in two sets of biopsy and surgical samples (different and identical cases). Over-expression of both genes is observed in surgically resected esophageal tumors, except *ZEB2* in the different cases. *$P<0.05$.
(TIF)

Figure S3 Expression levels of *TWIST1* in two sets of biopsy and surgical samples (different and identical cases). Over-expression of *TWIST1* is observed in surgically resected esophageal tumors. *$P<0.05$.
(TIF)

Figure S4 Schema of crosstalk between Hh and EMT signal pathways in esophageal cancers. The primary transcriptional factor GLI1 and an EMT regulator TWIST1 regulate another EMT regulator ZEB2, which activates any gene including membrane type receptors (*PDGFRA*, *EDNRA*, *CXCR4*, *VEGFR2*, and *TRKB*) [9].
(TIF)

Figure S5 Expression levels of *HIF1A*, *HIF1B*, *HIF2A*, and *LOXL2* in two sets of biopsy and surgical samples (different and identical cases). Over-expression of *HIF1A* and its target *LOXL2* is observed only in surgically resected esophageal tumors (different cases).
(TIF)

Figure S6 Expression levels of *NFKB1* and *TGFBR2* in two sets of biopsy and surgically resected tumor samples (different and identical cases) and in biopsy and surgically resected non-cancerous tissues (normal). Over-expression of *NFKB1* and *TGFBR2* is observed in all the sets of surgically resected samples. $*P<0.05$.
(TIF)

Table S1 219 up-regulated genes in 66 surgically resected esophageal tumors.
(DOC)

Table S2 716 up-regulated genes in 18 surgically resected esophageal tumors.
(DOC)

Table S3 Clinicopathological information of biopsy samples from different cases with esophageal squamous cell carcinoma.
(DOC)

Table S4 Clinicopathological information of surgical samples from different cases with esophageal squamous cell carcinoma.
(DOC)

Table S5 Clinicopathological information of biopsy and surgical samples from different cases with esophageal squamous cell carcinoma.
(DOC)

Acknowledgments

We gratefully thank Dr. Narikazu Boku, Dr. Hiroshi Sato, and Dr. Yasuhiro Tsubosa of Shizuoka Cancer Center for the pathological and clinical evaluation. We also thank Ms. Rie Komatsuzaki, Ms. Akemi Sugai, and Ms. Fumiko Chiwaki for their technical assistance.

Author Contributions

Conceived and designed the experiments: KA KM MM A. Ohtsu TY HS. Performed the experiments: KA TN AA. Analyzed the data: KA HS. Contributed reagents/materials/analysis tools: KM HI YT A. Ochiai NH HD MM A. Ohtsu. Wrote the paper: KA HS.

References

1. Kim C, Pik S (2010) Gene-expression-based prognostic assays for breast cancer. Nat Rev Clin Oncol 7: 340–347.
2. Fordor SP, Read JL, Pirrung MC, Stryer L, Lu AT, et al. (1991) Light-directed, spatially addressable parallel chemical synthesis. Science 251: 767–773.
3. Lockhart DJ, Dong H, Byrne MC, Follettie MT, Gallo MV, et al. (1996) Expression monitoring by hybridization to high-density ologonucleotide arrays. Nat Biothechnol 14: 1675–1680.
4. DeRisi J, Penland L, Brown PO, Bittner ML, Meltzer PS, et al. (1996) Use of a cDNA microarray to analyze gene expression patterns in human cancer. Nat Genet 14: 457–460.
5. Brown PO, Botstein D (1999) Exploring the new world of the genome with DNA microarrays. Nat Genet 21: 33–37.
6. Ishikura S, Nihei K, Ohtsu A, Boku N, Hironaka S, et al. (2003) Long-term toxicity after definitive chemoradiotherapy for squamous cell carcinoma of the thoracicesophagus. J Clin Oncol 21: 2697–2702.
7. Tachimori Y, Kanamori N, Uemura N, Hokamura N, Igaki H, et al. (2009) Salvage esophagectomy after high-dose chemoradiotherapy for esophageal squamous cell carcinoma. J Thorac Cardiovasc Surg 137: 49–54.
8. Ashida A, Boku N, Aoyagi K, Sato H, Tsubosa Y, et al. (2006) Expression profiling of esophageal squamous cell carcinoma patients treated with definitive chemoradiotherapy: clinical implications. Int J Oncol 28: 1345–1352.
9. Isohata N, Aoyagi K, Mabuchi T, Daiko H, Fukaya M, et al. (2009) Hedgehog and epithelial-mesenchymal transition signaling in normal and malignant epithelial cells of the esophagus. Int J Cancer 125: 1212–1221.
10. Sano M, Aoyagi K, Takahashi H, Kawamura T, Mabuchi T, et al. (2010) Forkhead box A1 transcriptional pathway in KRT7-expressing esophageal squamous cell carcinomas with extensive lymph node metastasis. Int J Oncol 36: 321–330.
11. Yang J, Weinberg RA (2008) Epithelial-mesenchymal transition: at the crossroads of development and tumor metastasis. Dev Cell 14: 818–829.
12. Thiery JP, Acloque H, Huang RY, Nieto MA (2009) Epithelial-mesenchymal transitions in development and disease. Cell 139: 871–890.
13. Yang MH, Wu MZ, Chiou SH, Chen PM, Chang SY, et al. (2008) Direct regulation of TWIST by HIF-1alpha promotes metastasis. Nat Cell Biol 10: 295–305.
14. Gort EH, van Haaften G, Verlaan I, Groot AJ, Plasterk RH, et al. (2008) The TWIST1 oncogene is a direct target of hypoxia-inducible factor-2alpha. Oncogene 27: 1501–1510.
15. Peinado H, del Carmen M, La Cruz I-D, Olmeda D, Csiszar K, et al. (2005) A molecular role for lysyl oxidase-like 2 enzyme in Snail regulation and tumor progression. EMBO J 24: 3446–3458.
16. Katoh M, Katoh M (2009) Integrative genomic analyses of ZEB2: Transcriptional regulation of ZEB2 based on SMADs, ETS1, HIF1alpha, POU/OCT, and NF-kappaB. Int J Oncol 34: 1737–1742.
17. Eoin PC, Edurne B, Katrina MC, Amandine G, Kathleen TF, et al. (2006) Prolyl hydroxylase-1 negatively regulates IκB kinase-β, giving insight into hypoxia-induced NF"Insert>Symbol,"kB activity. Proc Natl Acad Sci USA 103: 18154–18159.
18. Chengyin M, Sean FE, David HS, Gail ES (2008) NF-κB and epithelial to mesenchymal transition of cancer. J Cell Biochem 104: 733–744.
19. Cormac TT, Eoin PC (2009) The role of NF-κB in hypoxia-induced gene expression. Hypoxia and consequences. Ann NY Acad Sci 1177: 178–184.
20. Luthra R, Wu T-T, Luthra MG, Izzo J, Lopez-Alvarez E, et al. (2006) Gene expression profiling of localized esophageal carcinomas: association with pathologic response to preopererative chemoradiation. J Clin Oncol 24: 259–267.
21. Duong C, Greenawalt DM, Kowalczyk A, Ciavarella ML, Raskutti G, et al. (2007) Pretreatment gene expression profiles can be used to predict response to neoadjuvant chemoradiotherapy in esophageal cancer. Ann Surg Oncol 14: 3602–3609.
22. Izzo JG, Wu X, Wu T-T, Huang P, Lee JS, et al. (2009) Therapy-induced expression of NF-κB portends poor prognosis in patients with localized esophageal cancer undergoing preoperative chemoradiation. Dis Esophagus 22: 127–132.
23. Maher SG, Gillham CM, Duggan SP, Smyth PC, Miller N, et al. (2009) Gene expression analysis of diagnostic biopsies predicts pathological response to neoadjuvant chemoradiotherapy of esophageal cancer. Ann Surg 250: 729–737.
24. Aoyagi K, Tatsuta T, Nishigaki M, Akimoto S, Tanabe C, et al. (2003) A faithful method for PCR-mediated global mRNA amplification and its integration into microarray analysis on laser-captured cells. Biochem Biophys Res Commun 300: 915–920.
25. Fukaya M, Isohata N, Ohta H, Aoyagi K, Ochiya T, et al. (2006) Hedgehog signal activation in gastric pit cell and in diffuse-type gastric cancer. Gastroenterology 131: 14–29.
26. Nakamura N, Kobayashi K, Nakamoto M, Kohno T, Sasaki H, et al. (2006) Identification of tumor markers and differentiation markers for molecular diagnosis of lung adenocarcinoma. Oncogene 25: 4245–4255.
27. Nishigaki M, Aoyagi K, Danjoh I, Fukaya M, Yanagihara K, et al. (2005) Discovery of aberrant expression of R-RAS by cancer-linked DNA hypomethylation in gastric cancer using microarrays. Cancer Res 65: 2115–2124.
28. Saeki N, Kim DH, Usui T, Aoyagi K, Tatsuta T, et al. (2007) GASDERMIN, suppressed frequently in gastric cancer, is a target of LMO1 in TGF-β-dependent apoptotic signalling. Oncogene 26: 6488–6498.
29. Eisen MB, Spellman PT, Brown PO, Botstein D (1998) Cluster analysis and display of genome-wide expression patterns. Proc Natl Acad Sci USA 95: 14863–14868.

The Laryngoscope

Diagnosis of the Extent of Advanced Oropharyngeal and Hypopharyngeal Cancers by Narrow Band Imaging With Magnifying Endoscopy

Hiroki Matsuba, MD; Chikatoshi Katada, MD, PhD; Takashi Masaki, MD; Meijin Nakayama, MD, PhD; Tabito Okamoto, MD; Noboru Hanaoka, MD, PhD; Satoshi Tanabe, MD, PhD; Wasaburo Koizumi, MD, PhD; Makito Okamoto, MD, PhD; Manabu Muto, MD, PhD

Objectives/Hypothesis: Narrow band imaging combined with magnifying endoscopy (NBI-ME) is useful for the detection of superficial cancer in the oropharynx, hypopharynx, and esophagus. We used NBI-ME to evaluate the frequency of superficial cancer spread (SCS) contiguous with advanced oropharyngeal and hypopharyngeal cancers and esophageal cancers.

Study Design: Retrospective.

Methods: We retrospectively studied 45 patients with oropharyngeal and hypopharyngeal cancer and 44 with esophageal cancer who underwent NBI-ME from October 2006 through April 2009. The following variables were evaluated: 1) the frequency of SCS contiguous with advanced oropharyngeal and hypopharyngeal cancer and esophageal cancer, and 2) the influence of SCS contiguous with advanced oropharyngeal and hypopharyngeal cancer on clinical T category and clinical stage.

Results: SCS contiguous with the primary tumor was found in 49% (22/45) of the patients with advanced oropharyngeal and hypopharyngeal cancer and in 52% (23/44) of those with advanced esophageal cancer. When SCS contiguous with the primary tumor was included in the evaluation of tumor size in advanced oropharyngeal and hypopharyngeal cancer, the clinical T category and clinical stage were revised in 20% (9/45) and 4% (2/45) of patients, respectively; SCS was $\leq$2 cm in 64% of cases (14/22) and between >2 cm and $\leq$4 cm in 36% (8/22).

Conclusions: NBI-ME should be included in the pretreatment diagnostic work-up to evaluate lesion extent and decide optimal surgical margins and radiation fields in patients with advanced oropharyngeal and hypopharyngeal cancer.

Key Words: Narrow band imaging, magnifying endoscopy, lesion extent, head and neck cancer.

Level of Evidence: 3b

***Laryngoscope*, 121:753–759, 2011**

INTRODUCTION

The advent of narrow band imaging (NBI) and high-resolution magnifying endoscopy (ME) has facilitated the detection of superficial cancer in the oropharynx, hypopharynx, and esophagus.[1–6] These techniques have also enabled the lateral spread of superficial cancer contiguous with advanced oropharyngeal, hypopharyngeal, and esophageal tumors to be visualized, allowing an accurate evaluation of lesion extent, which is essential for setting surgical margins and radiation fields. We used NBI combined with ME (NBI-ME) to examine the frequency of superficial cancer spread (SCS) contiguous with advanced oropharyngeal and hypopharyngeal cancers and esophageal cancers.

From the Department of Otorhinolaryngology (H.M., T.M., M.N., T.O., M.O.), Department of Gastroenterology (C.K., N.H., S.T., W.K.), Kitasato University School of Medicine, Sagamihara, the Department of Gastroenterology and Hepatology (M.M.), Kyoto University Graduate School of Medicine, Kyoto, Japan.

Editor's Note: This Manuscript was accepted for publication November 17, 2010.

The authors have no funding, financial relationships, or conflicts of interest to disclose.

Send correspondence to Chikatoshi Katada, MD, PhD, Department of Gastroenterology, Kitasato University School of Medicine, 1-15-1 Kitasato, Minami- ku, Sagamihara 252-0374, Japan.
E-mail: ckatada@med.kitasato-u.ac.jp

DOI: 10.1002/lary.21553

MATERIALS AND METHODS

We retrospectively studied 45 patients with oropharyngeal and hypopharyngeal cancer and 44 with esophageal cancer who underwent NBI-ME at Kitasato University Hospital from October 2006 through April 2009. All patients met all of the following criteria: 1) no previous treatment for head and neck cancer or esophageal cancer, 2) a histopathological diagnosis of squamous-cell carcinoma, 3) advanced cancer, 4) computed tomography (CT) had been performed, and 5) chromoendoscopy with Lugol's iodine solution had been performed (only for patients with advanced esophageal cancer).

The following variables were evaluated: 1) the frequency of SCS contiguous with advanced oropharyngeal and hypopharyngeal cancer and esophageal cancer, and 2) the influence of SCS contiguous with advanced oropharyngeal and hypopharyngeal cancer on clinical T category and clinical stage. In this study, we performed NBI with a high-definition videoendoscopy system (with a CV-260SL processor and a CLV-260SL light source; Olympus Optical Co., Ltd., Tokyo, Japan) and an optical magnifying endoscope with a system that could magnify objects up to 80 times (GIF type H260Z videoendoscope; Olympus). A 1.5% solution of Lugol dye was used to perform chromoendoscopy according to the Lugol dye-staining method (Lugol

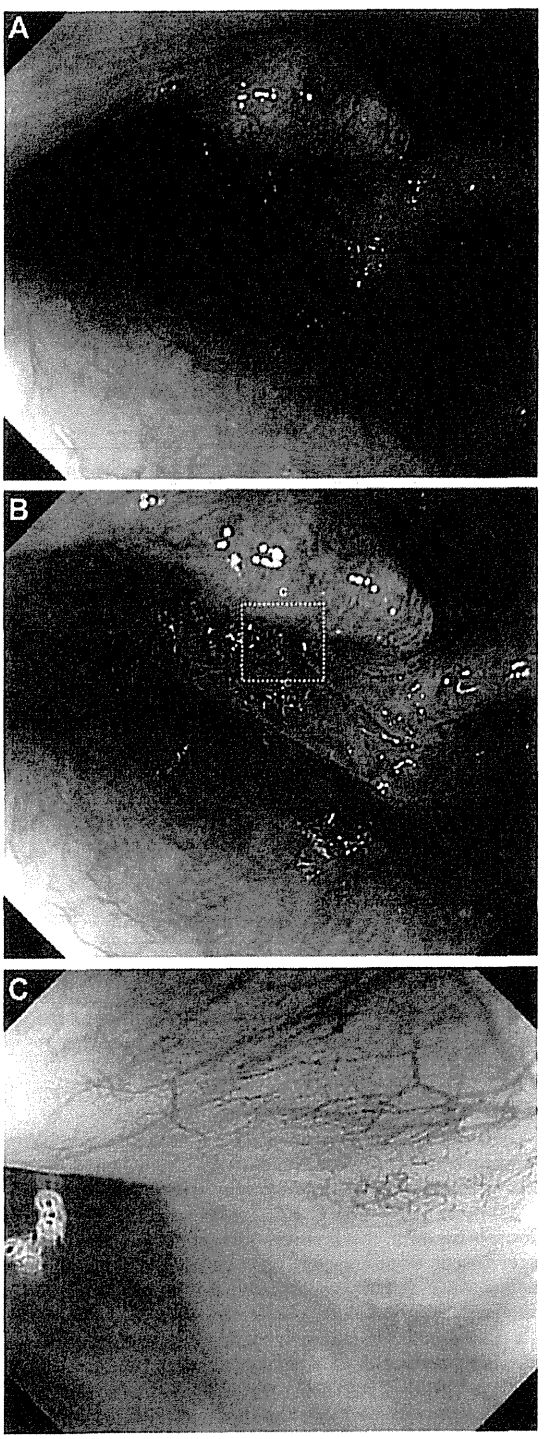

Fig. 1. Normal mucosa in the left postcricoid area. (A) White light endoscopy. (B) Narrow band imaging. (C) Narrow band imaging-magnifying endoscopy, showing a regular microvascular pattern beneath the epithelium.

chromoendoscopy)[7] in all patients with esophageal cancer. Examinations in patients with advanced oropharyngeal and hypopharyngeal cancer were performed in the following order: white light endoscopy, NBI endoscopy, and NBI-ME. In patients with advanced esophageal cancer, examinations were done in the following order: white light endoscopy, NBI endoscopy, NBI-ME, and Lugol chromoendoscopy. Superficial cancer was defined as a lesion with high-grade intraepithelial neoplasia or microinvasive cancer as diagnosed endoscopically according to the World Health Organization classification of tumors.[8] Advanced cancer was defined as a lesion with deeper invasion. Superficial cancer contiguous with the primary tumor was diagnosed endoscopically on the basis of 1) a well-demarcated area and 2) an irregular microvascular pattern.[2–6] Endoscopic images were reviewed by an otolaryngological endoscopist (h.m.) and a gastrointestinal endoscopist (c.k.). Clinical T category and clinical stage were assessed according to the 7th edition of the International Union Against Cancer (UICC) tumor-node-metastasis (TNM) staging system.[9] At the time of endoscopy, we estimated the size of the lesion by placing biopsy forceps (FB-25K-1; Olympus) alongside the lesion; the fully opened cup of the forceps was 6 mm in diameter.

Normal mucosa in the left postcricoid area is shown in Figure 1. On white light endoscopy (Fig. 1A) and NBI (Fig. 1B), a regular microvascular pattern beneath the epithelium was difficult to identify. However, NBI-ME (Fig. 1C) clearly showed a regular microvascular pattern beneath the epithelium. Advanced hypopharyngeal cancers arising in the left postcricoid area are shown in Figure 2 and Figure 3.

In the first case, the tumor was nonulcerative and was situated mainly in the submucosa. SCS extended from the surface of the lesion to its distal border. The greatest tumor dimension was 15 mm in the transverse plane (Fig. 2A) and 22 mm in the coronal plane (Fig. 2B) on CT, and about 25 mm on white light endoscopy (Fig. 2C). Therefore, the lesion was classified as a clinical T2 tumor. NBI showed a well-demarcated, brownish area on the surface of the lesion (Fig. 2D). NBI-ME revealed an irregular microvascular pattern (Fig. 2E). SCS about 10 mm in diameter was contiguous with the anal side of the primary tumor (Fig. 2F), but there was no upgrade of the clinical T category.

In the next case, the tumor was ulcerative and accompanied by SCS only at the border of the lesion. The greatest tumor dimension was 11 mm in the transverse plane (Fig. 3A) and 24 mm in the coronal plane (Fig. 3B) on CT, and about 25 mm on white light endoscopy (Fig. 3C). The lesion was classified as a clinical T2 tumor. NBI showed a well-demarcated, brownish area in the lateral wall (Fig. 3D). NBI-ME revealed an irregular microvascular pattern. SCS extended for about 30 mm from the postcricoid area to the lateral wall via the pyriform sinus and was contiguous with the primary tumor (Fig. 3E). When this spread was included in the evaluation, the clinical T category was upgraded from T2 to T3.

A case of advanced esophageal cancer is shown in Figure 4. White light endoscopy revealed advanced esophageal cancer, occupying half of the circumference of the esophagus (Fig. 4A). NBI showed a well-demarcated, brownish area at the border of the primary tumor (Fig. 4B). NBI-ME revealed an irregular microvascular pattern (Fig. 4C). SCS as an unstained area at the border of the primary tumor was seen on Lugol chromoendoscopy (Fig. 4D). Because the clinical T category of esophageal cancer is based on the depth of tumor invasion, the presence of SCS contiguous to the primary tumor does not alter the classification of clinical T category.

RESULTS

Table I shows the demographic characteristics of the patients. The study group comprised 78 men (88%) and 11 women (12%), with a mean age (±standard

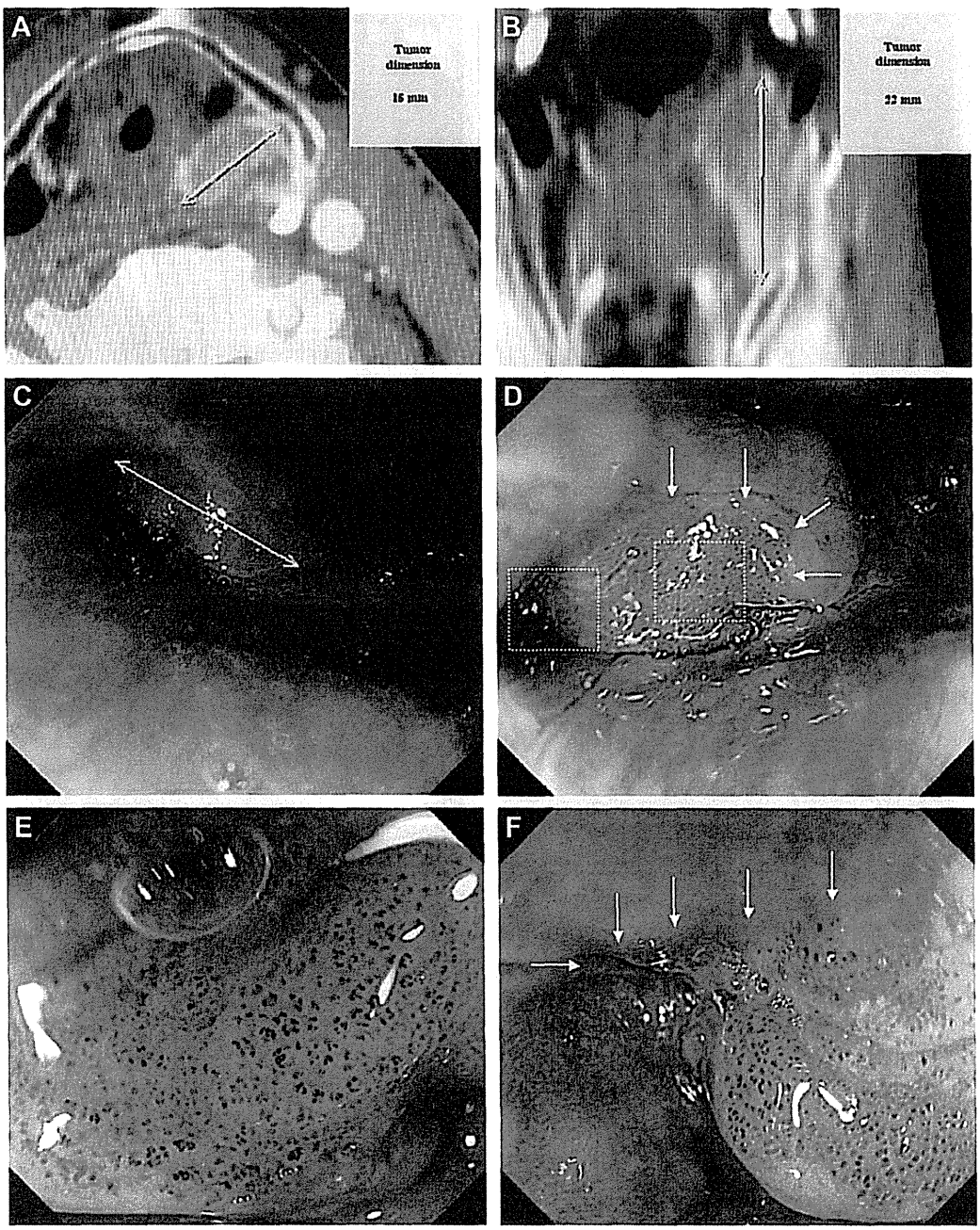

Fig. 2. Advanced hypopharyngeal cancer arising in the left postcricoid area. The tumor was nonulcerative and situated mainly in the submucosa. Superficial cancer spread extended from the surface of the lesion to its distal border. (A) The greatest tumor dimension was 15 mm in the transverse plane on computed tomography (CT). (B) The greatest tumor dimension was 22 mm in the coronal plane on CT. (C) The greatest tumor dimension was about 25 mm on white light endoscopy. (D) Narrow band imaging showed a well-demarcated, brownish area (arrows). (E) Narrow band imaging-magnifying endoscopy revealed an irregular microvascular pattern. (F) Superficial cancer spread about 10 mm in diameter was contiguous with the anal side of the primary tumor (arrows).

deviation) of 66 ± 8.7 years. Among six patients (7%) with oropharyngeal cancer, the primary tumor was located in the anterior wall in four patients (5%), the lateral wall in one patient (1%), and the posterior wall in one patient (1%). Among 39 patients (44%) with hypopharyngeal cancer, the primary tumor was located in the pyriform sinus in 22 patients (25%), the postcricoid area in nine patients (10%), and the posterior wall in eight patients (9%). A total of 44 patients (49%) had primary esophageal cancer.

SCS contiguous with the primary tumor was found in 49% (22/45) of the patients with advanced oropharyngeal and hypopharyngeal cancer and in 52% (23/44) of those with advanced esophageal cancer. In patients with

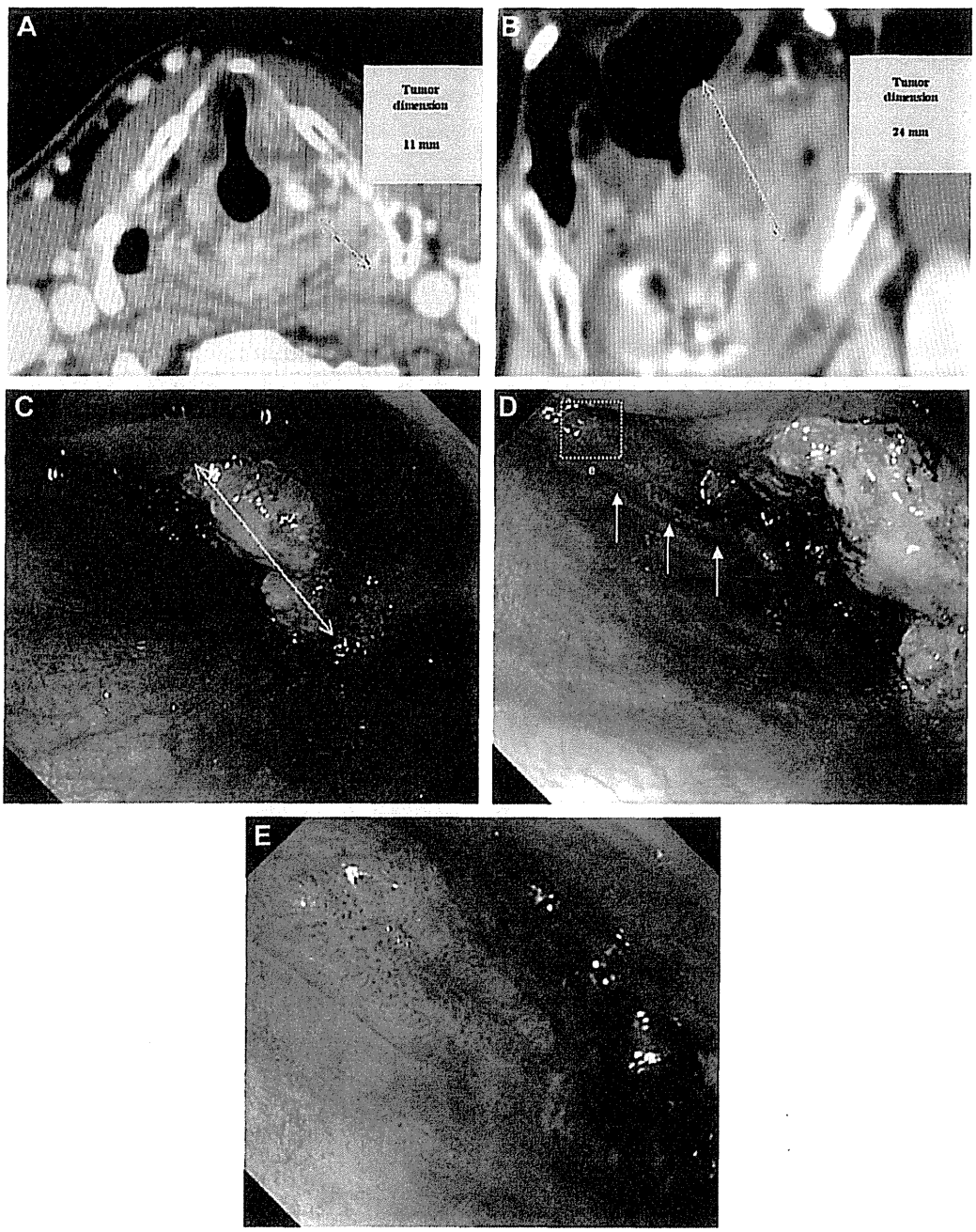

Fig. 3. Advanced hypopharyngeal cancer arising in the left postcricoid area. The tumor was ulcerative, and superficial cancer spread was present only at its border. (A) The greatest tumor dimension was 11 mm in the transverse plane on computed tomography (CT). (B) The greatest tumor dimension was 24 mm in the coronal plane on CT. (C) The greatest tumor dimension was about 25 mm on white light endoscopy. (D) Narrow band imaging showed a well-demarcated, brownish area (arrows). (E) Narrow band imaging-magnifying endoscopy revealed an irregular microvascular pattern. Superficial cancer spread extended for about 30 mm from the postcricoid area to the lateral wall via the pyriform sinus and was contiguous with the primary tumor.

advanced esophageal cancer, the ability to detect SCS was similar for Lugol chromoendoscopy and NBI-ME. The clinical T category was revised in nine patients (20%) who had advanced oropharyngeal and hypopharyngeal cancer; it was upgraded from T1 to T2 in two patients (4%) and from T2 to T3 in seven patients (16%). The clinical stage was revised in two patients (4%); one patient (2%) was upgraded from stage I to II, and one patient (2%) was upgraded from stage II to III. In patients with advanced esophageal cancer, there was no change in clinical T category or in clinical stage (Table II).

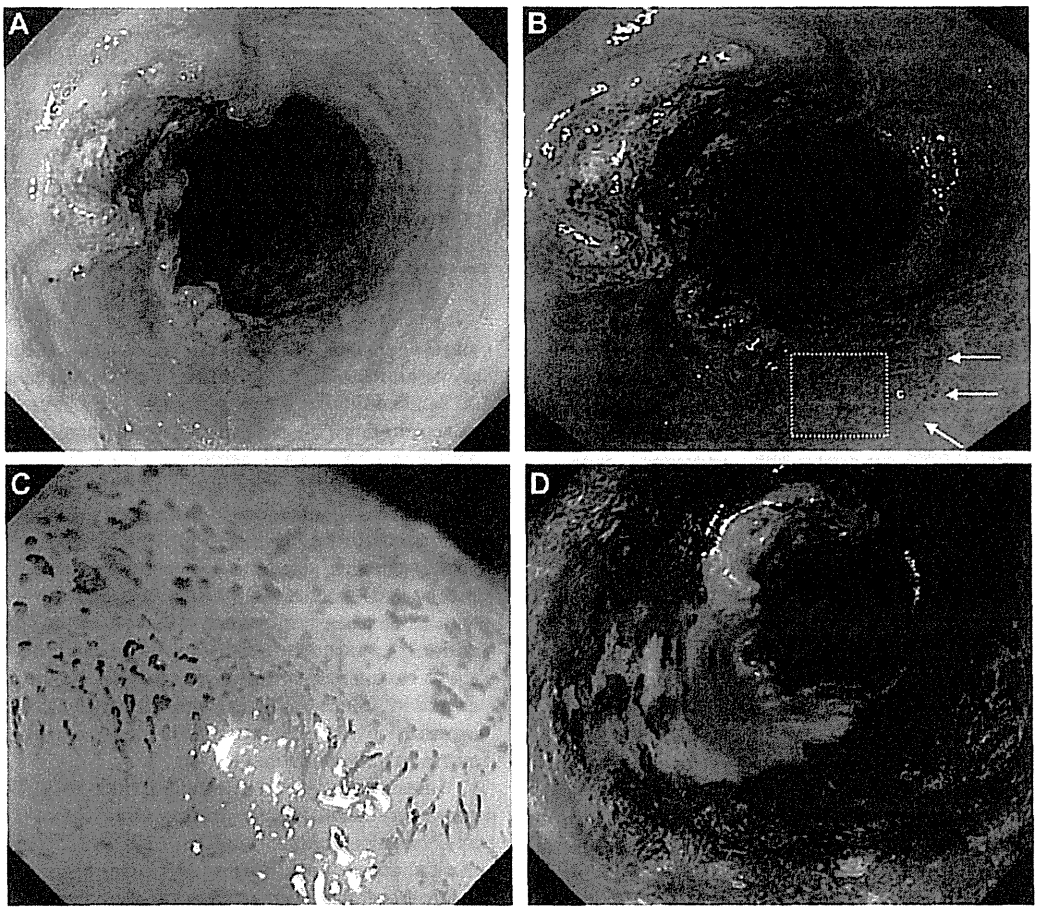

Fig. 4. Advanced esophageal cancer. (A) White light endoscopy revealed advanced esophageal cancer. (B) Narrow band imaging showed a well-demarcated, brownish area at the border of the primary tumor (arrows). (C) Narrow band imaging-magnifying endoscopy revealed an irregular microvascular pattern. (D) Superficial cancer spread appeared as an unstained area at the border of the primary tumor on Lugol chromoendoscopy.

TABLE I.
Patient and Lesion Demographics (n = 89).

Gender, no. (%)	
Male	78 (88)
Female	11 (12)
Age, mean ± SD, yr	66 ± 8.7
Range, yr	45–89
Site of primary cancer, no. (%)	
Oropharynx	6 (7)
Anterior wall	4 (5)
Lateral wall	1 (1)
Posterior wall	1 (1)
Hypopharynx	39 (44)
Pyriform sinus	22 (25)
Postcricoid area	9 (10)
Posterior wall	8 (9)
Esophagus	44 (49)

SD = standard deviation.

The dimensions of SCS contiguous with the primary tumor are summarized in Table III. In advanced oropharyngeal and hypopharyngeal cancer, SCS was ≤2 cm in 64% of cases (14/22), between >2 cm and ≤4 cm in 36% (8/22), and >4 cm in 0% (0/22). In advanced esophageal cancer, SCS was ≤2 cm in 52% (12/23) of cases, between >2 cm and ≤4 cm in 30% (7/23), and >4 cm in 17% (4/23). The size of SCS did not differ between patients with advanced oropharyngeal and hypopharyngeal cancer and those with advanced esophageal cancer ($P = .237$).

DISCUSSION

A nationwide survey conducted by the Japan Society for Head and Neck Cancer in 2005 reported that no patient with oropharyngeal and hypopharyngeal cancer had carcinoma in situ at initial presentation, suggesting that is it very difficult to visually confirm superficial cancer in the oropharynx and hypopharynx.[10] Laryngoscopy was conventionally used to detect oropharyngeal and hypopharyngeal cancer. However, the advent of NBI-ME has markedly improved the ability to visualize superficial cancer,[2–6] facilitating the diagnosis of SCS

contiguous with advanced cancer. In the present study of SCS contiguous with advanced oropharyngeal cancer and hypopharyngeal cancer, the rates of clearly visualizing "well-demarcated areas" and "irregular microvascular patterns," considered endoscopic characteristics of superficial cancer, on white light endoscopy, NBI, and NBI-ME were 23% (5/22), 82% (18/22), and 100% (22/22) for the former, respectively; and 14% (3/22), 77% (17/22), and 100% (22/22) for the latter, respectively. Therefore, well-demarcated areas and irregular microvascular patterns of SCS were better visualized by NBI and NBI-ME than by white light endoscopy. Furthermore, NBI-ME allowed definitive visualization of both of these characteristics. Muto et al. reported that the sensitivities and accuracies for the diagnosis of superficial cancer in the oropharynx and hypopharynx were 7.7% and 62.9% for white light endoscopy, respectively, as compared with 100% and 86.7% for NBI-ME, respectively. For the diagnosis of superficial esophageal cancer, the sensitivities and accuracies were 55.2% and 56.5% for white light endoscopy, respectively, and 97.2% and 88.9% for NBI-ME, respectively.[5] In the present study, a histopathological diagnosis could be made in 29 (64%) of 45 cases of SCS that were diagnosed endoscopically (14 cases of oropharyngeal cancer and hypopharyngeal cancer and 15 cases of esophageal cancer). However, superficial cancer was histologically confirmed in all cases. These findings indicate that the diagnostic accuracy of NBI-ME for SCS is extremely high.

Lugol chromoendoscopy has been used to diagnose lesion extent in patients with esophageal cancer,[7] but cannot be used to examine the oropharynx and hypopharynx because of the high risk of aspiration and the strong local irritation caused by iodine. In our study, all cases of SCS contiguous with advanced esophageal cancer detected on Lugol chromoendoscopy were also visualized on NBI. This finding suggested that NBI is also likely to be useful for the confirmation of SCS contiguous with advanced oropharyngeal and hypopharyngeal cancer, which cannot be evaluated on Lugol chromoendoscopy. In our study, SCS was associated with 49% of advanced oropharyngeal and hypopharyngeal cancers and 52% of advanced esophageal cancers (i.e., about one half of the patients with each type of cancer). To our knowledge, this is the first time similar frequencies of SCS contiguous with the primary tumor in patients with advanced oropharyngeal and hypopharyngeal cancer, and those with advanced esophageal cancer were reported. Therefore, we believe that our results are very important. Moreover, in 18% (8/45) of patients with advanced oropharyngeal and hypopharyngeal cancer, SCS contiguous with the primary tumor exceeded 2 cm. We therefore consider NBI-ME to be essential for the determination of appropriate surgical margins and radiation fields.

TABLE II.
Frequency of Superficial Cancer Spread Contiguous With Primary Tumor and Effects on Clinical T Category and Clinical Stage.

	Advanced Oropharyngeal/ Hypopharyngeal Cancer (n = 45)	Advanced Esophageal Cancer (n = 44)
Frequency of superficial cancer spread, no. (%)		
NBI-ME	22 (49)	23 (52)
Lugol chromoendoscopy	NE	23 (52)
Frequency of changes in clinical T category, no. (%)	9 (20)	0 (0)
From clinical T1 to T2	2 (4)	
From clinical T2 to T3	7 (16)	
Frequency of changes in clinical stage, no. (%)	2 (4)	0 (0)
From clinical stage I to II	1 (2)	
From clinical stage II to III	1 (2)	

NBI = narrow band imaging; ME = magnifying endoscopy; NE = not evaluated.

TABLE III.
Dimensions of Superficial Cancer Spread.

	Advanced Oropharyngeal/ Hypopharyngeal Cancer (n = 22)	Advanced Esophageal Cancer (n = 23)	*P* Value*
0 cm to ≤2 cm	14 (64%)	12 (52%)	
>2 cm to ≤4 cm	8 (36%)	7 (30%)	
>4 cm	0 (0%)	4 (17%)	.237

*Calculated using Mann-Whitney *U* test.

Because the 7th edition of the UICC TNM staging system does not include contiguous SCS as a staging factor,[9] we examined whether clinical T category and clinical stage were altered by including contiguous SCS in the greatest dimension of the primary tumor. In esophageal cancer, the clinical T category is determined by the depth of primary tumor invasion.[9] Consequently, the presence of SCS contiguous with the primary tumor does not change the clinical T category. In contrast, the clinical T category of oropharyngeal and hypopharyngeal cancer depends on the greatest dimension of the primary tumor.[9] The inclusion of SCS contiguous with the primary tumor in the evaluation of tumor size may thus alter the clinical T category, potentially affecting the clinical stage grouping. When we included SCS contiguous with the primary tumor in the calculation of the greatest tumor dimension in patients with oropharyngeal and hypopharyngeal cancer, the clinical T category was upgraded in 20% of cases. However, the effect on clinical stage was minimal. Clinical T categories were decided before it was possible to clinically evaluate SCS contiguous with the primary tumor. With improved diagnostic techniques, contiguous SCS can now be evaluated. Therefore, a discussion of whether to include contiguous SCS in the evaluation of clinical T category now appears to be warranted.

CONCLUSION

In this study, advanced oropharyngeal and hypopharyngeal cancer is frequently associated with contiguous SCS. NBI-ME should be included in the pretreatment diagnostic work-up to evaluate lesion extent

and decide optimal surgical margins and radiation fields.

BIBLIOGRAPHY

1. Gono K, Obi T, Yamaguchi M, et al. Appearance of enhanced tissue features in narrow-band endoscopic imaging. *J Biomed Opt* 2004;9: 568–577.
2. Muto M, Nakane M, Katada C, et al. Squamous cell carcinoma in situ at oropharyngeal and hypopharyngeal mucosal sites. *Cancer* 2004;101: 1375–1381.
3. Nonaka S, Saito Y. Endoscopic diagnosis of pharyngeal carcinoma by NBI. *Endoscopy* 2008;40:347–351.
4. Katada C, Nakayama M, Tanabe S, et al. Narrow band imaging for detecting metachronous superficial oropharyngeal and hypopharyngeal squamous cell carcinomas after chemoradiotherapy for head and neck cancers. *Laryngoscope* 2008;118:1787–1790.
5. Muto M, Minashi K, Yano T, et al. Early detection of superficial squamous cell carcinoma in the head and neck region and esophagus by narrow band imaging: a multicenter randomized controlled trial. *J Clin Oncol* 2010;28:1566–1572.
6. Katada C, Tanabe S, Koizumi W, et al. Narrow band imaging for detecting superficial squamous cell carcinoma of the head and neck in patients with esophageal squamous cell carcinoma. *Endoscopy* 2010;42:185–190.
7. Inoue H, Rey JF, Lightdale C. Lugol chromoendoscopy for esophageal squamous cell cancer. *Endoscopy* 2001;33:75–79.
8. Hamilton SR, Aaltonen LA, eds. *World Health Organization Classification of Tumors. Pathology and Genetics of Tumors of the Digestive System.* Lyon, France: IARC Press; 2000:9–30.
9. Sobin LH, Gospondarowicz MK, Wittekind CH. *International Union Against Cancer (UICC). TNM Classification of Malignant Tumours.* 7th ed. New York, NY: Wiley; 2010:30–38.
10. *Japan Society for Head and Neck Cancer. General Rules for Clinical Studies on Head And Neck Cancer.* Tokyo, Japan: Kanehara Syuppan; 2005:73–95.

Commentary

Although rare, fibrovascular polyps of the esophagus (FVPEs) comprise most of this organ's benign intraluminal tumor-like lesions. FVPE are composed of fibrous tissue, adipose tissue, and vascular structures and are covered by normal squamous epithelium. Depending on which histologic components predominate, FVPEs also may be referred to as lipomas, fibromas, fibrolipomas, fibromyxomas, and fibroepithelial polyps. With an average length of 15 cm, FVPEs arise from just below the cricopharyngeus muscle in the area known as Killian's or Laimer's triangle. When small, these lesions are asymptomatic. Symptoms only develop when FVPEs reach a large size and include dysphagia, regurgitation of the polyp into the mouth, bleeding, dyspnea, stridor, wheezing, choking, and even asphyxiation. One reported case described a patient who regurgitated a giant FVPE into his mouth and captured it between his teeth until it could be removed endoscopically. Upper GI series and endoscopy can be diagnostic, but an FVPE may be missed at endoscopy because the polyp is covered by normal mucosa and can be highly mobile. Surgical excision or endoscopic resection is definitive treatment, but care must be taken to ensure that the prominent vessels in the stalk are completely ligated or coagulated. The stalk should be completely excised or recurrence is possible. I think of the folk album Arkansas Traveler, on which Michelle Shocked popularized the now classic tune "Come a Long Way" singing "I come a long way, I come a long way and never even left LA." Well these polyps also come a long way, but never leave the area of the cricopharyngeus. If regurgitated out from their point of residence, like Michelle, they leave the patient—and the physician—shocked.

Lawrence J. Brandt, MD,
Associate Editor for Focal Points

A case of esophageal ulcer caused by alendronate sodium tablets

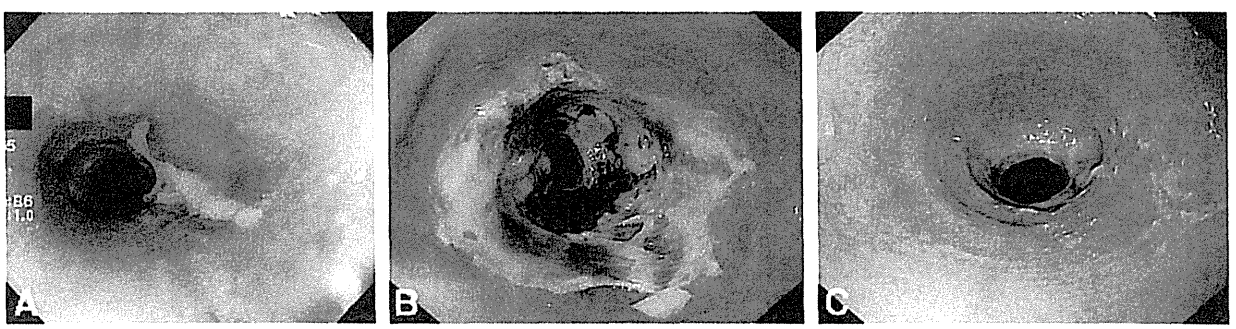

A 75 year old woman was referred to our hospital with dysphagia. Esophagoscopic examination revealed a shallow ulceration at the upper esophageal region (**A**). She had no history of esophageal disorder.

The ulceration gradually improved without treatment, but 6 months later a follow-up esophagoscopic examination showed a circumferential ulceration with severe stricture in the same region (**B**). Because she had been taking alendronate sodium weekly to prevent osteoporosis for 2 years before presentation, we recommended it be discontinued. The esophageal ulcer progressively healed (**C**); however, 7 sessions of endoscopic balloon dilation over 6 months were needed to relieve her dysphagia. Clinicians should consider the possibility of adverse effects from alendronate sodium tablets in the appropriate patient with esophageal ulceration.

DISCLOSURE

All authors disclosed no financial relationships relevant to this publication.

Kosuke Ueda, MD, Manabu Muto, MD, PhD, Tsutomu Chiba, MD, PhD, *Department of Gastroenterology and Hepatology, Graduate School of Medicine, Kyoto University, Kyoto, Japan*

doi:10.1016/j.gie.2010.11.039

Commentary

Alendronate sodium is a selective inhibitor of osteoclast-mediated bone resorption that increases bone mass, decreases vertebral fractures, and treats postmenopausal osteoporosis. Before its caustic effects on the upper GI tract were well appreciated, it was also the endocrinologist's contribution to endoscopy revenues. In early postmarket studies of alendronate, comprising nearly half a million patients, up to 25% of the drug's reported adverse events were from severe esophageal injury, primarily chemical esophagitis. Biopsy of the involved mucosa often shows polarizable crystalline material and multinucleated giant cells characteristic of pill-related injury. Alendronate should only be taken in the upright position, usually on arising for the day, and with 6 to 8 oz of water. Failure to adhere to this morning ritual may increase the risk of esophageal misadventure. Although this second-generation uncoated monosodium salt was designed, with some success, to maximize solubility and minimize esophageal mucosal adherence, retained tablets still can cause circumferential ulceration focally or throughout the esophagus. Although these changes can be persistent, strictures requiring repeated dilation are rare. What makes this case hard to swallow is the severity of the drug toxicity despite taking it as directed.

David Robbins, MD, MSc,
Assistant Editor for Focal Points

Partially migrated gastric ring after transected banded vertical gastric bypass

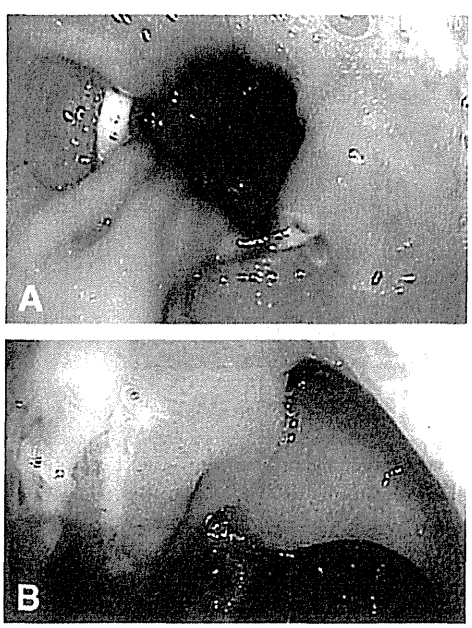

A 59-year-old man who had had bariatric surgery 4 years previously presented with maroon stools and dizziness. The patient was taking a nonsteroidal anti-inflammatory drug (NSAID). He was found to have orthostatic hypotension and tachycardia with normocytic anemia (hemoglobin 7 g/dL; normal 14-18 g/dL); blood test results were otherwise normal. EGD revealed a small gastric pouch that led into the small intestine. A ring that had partially eroded through the stomach wall was identified (**A**). The patient previously had a transected banded vertical gastric bypass, during which a silastic ring was placed around the gastric pouch proximal to the gastrojejunal anastomosis. A clean-based ulcer (**B**) also was found on the jejunal side of the anastomosis, without active bleeding or high-risk stigmata. NSAID therapy was discontinued, and the patient began therapy with omeprazole and was discharged.